Respiratory Physiology & Neurobiology 241 (2017) 62–71

Contents lists available at ScienceDirect

Respiratory Physiology & Neurobiology

journal homepage: www.elsevier.com/locate/resphysiol

# The Roughton-Forster equation for $DL_{CO}$ and $DL_{NO}$ re-examined

M.-Y. Kang[a], D. Grebenkov[a], H. Guénard[b], I. Katz[c,d], B. Sapoval[a,*]

[a] Physique de la Matière Condensée, CNRS, Ecole Polytechnique, 91128 Palaiseau, France
[b] Laboratoire de Physiologie, Université Bordeaux 2, 33076 Bordeaux, France
[c] Medical R&D, Air Liquide Santé International, Centre de Recherches Paris-Saclay, 78534 Jouy-en-Josas, France
[d] Department of Mechanical Engineering, Lafayette College, Easton, PA 18042, USA

ARTICLE INFO

*Article history:*
Received 22 July 2016
Received in revised form
19 December 2016
Accepted 28 December 2016
Available online 31 December 2016

*Keywords:*
DLCO
DLNO
Roughton and Forster
Capillary volume

ABSTRACT

Roughton and Forster (RF) proposed to split the lung diffusing capacity into two contributions describing first, diffusion to red blood cells (RBC), and second, capture by diffusion from the RBC surface and reaction with haemoglobin. Solving the diffusion-reaction equations for simplified capillary-RBC structures, we investigate the RF interpretation. This reveals first that the conventional extrapolation to zero pressure of 1/DLCO on $PO_2$ is not a correct measure of the diffusive component. Consequently the capillary volumes deduced from this extrapolation are erroneous. Secondly, capture mechanisms are different for CO and NO: while DLCO characterizes "volume absorption" in the RBC and is correlated with hematocrit, DLNO quantifies "surface absorption" and provide information about the morphology of the space between the alveolar surface and the RBC surfaces. In conclusion, the RF approach may lead to erroneous physiological interpretations of DLCO; nevertheless, the measurement of DLCO and DLNO bring different types of information that give the potential for a better understanding of respiratory diseases.

© 2017 The Authors. Published by Elsevier B.V. This is an open access article under the CC BY-NC-ND license (http://creativecommons.org/licenses/by-nc-nd/4.0/).

## 1. Introduction

The transport and capture of gaseous molecules by blood is a major process for life. As such, the quantitative understanding of oxygen respiration has been a primary scientific quest since Lavoisier in the late 18th century. Furthermore, the capture of carbon monoxide (CO), and more recently of nitric oxide (NO), has been studied for several reasons: First, to interpret the so-called diffusing capacity of CO (introduced by Marie Krogh in 1915 to study oxygen diffusion) and NO (Guénard et al., 1987; Borland and Higenbottam 1989) that is used in standard lung function tests. The quantification of CO capture is also important to assess the risks for accidental intoxication, smoking and environmental effects. Furthermore, there has been an interest in understanding the possible use of CO as an anti-inflammatory drug (Motterlini and Otterbein, 2010; Ryter and Choi, 2013). NO was identified as the endothelial derived relaxing factor (Furchgott and Zawadzki, 1980; Ignarro et al., 1987; Palmer et al., 1987). The vaso-relaxing effect of NO is used, through drugs acting as NO donors, for vasodilatation in some specific indications (Frostell et al., 1991; Griffiths and Evans, 2005; Checchia et al., 2012). Apart from its medical application, NO is also a common air pollutant in the air, coming from cigarette smoke, fuel consumption or nitrate used as fertilizer in agriculture.

Gas capture involves several steps each with a distinctive time scale. A schematic is shown in Fig. 1. The transport of gas molecules starts in the alveoli with gas concentration $C_g$. The concentration in the membrane on the other side of the alveolar-capillary interface is $\alpha C_g$, where $\alpha$ is the dimensionless gas to liquid partition ratio (Foucquier et al., 2013). The dissolution process occurs very rapidly, essentially instantaneously relative to the other time scales. The fact that the dissolution step is very rapid as compared to diffusion and reaction was used to understand quantitatively oxygen capture (Foucquier et al., 2013; Kang et al., 2015).

From the internal interface, each molecule from each location follows random paths (Brownian diffusion) through the membrane and the plasma into the red blood cell (RBC) cytoplasm to reach the haemoglobin (Hb) molecules and finally to react with them. A few of these Brownian trajectories reaching two small volume elements, $i$ and $j$, inside a RBC are illustrated in blue and green in Fig. 1. In each volume element $dV$ inside the RBC, Hb molecules trap CO (or NO) with a

$$\text{Reactive flux} = \frac{C_I}{\tau} dV \tag{1}$$

where $C_I$ is the concentration of the molecules to be trapped by haemoglobin inside the RBC and $1/\tau$ is the pseudo first-order rate constant (assuming $HbO_2$ in excess). This rate can be deduced from

* Corresponding author.
*E-mail address:* bernard.sapoval@polytechnique.edu (B. Sapoval).

http://dx.doi.org/10.1016/j.resp.2016.12.014
1569-9048/© 2017 The Authors. Published by Elsevier B.V. This is an open access article under the CC BY-NC-ND license (http://creativecommons.org/licenses/by-nc-nd/4.0/).

**List of symbols**

| | |
|---|---|
| $Cg$; $C_E$; $C_I$ | Respectively, concentrations of CO or NO in gas, in membrane-plasma external to RBCs, and inside RBCs |
| $D_{CO}$; $D_{NO}$ | Diffusion coefficients of CO and NO in plasma in $cm^2/s$ |
| $DL_{CO}$; $DL_{NO}$ | Lung diffusing capacity for CO and NO in $ml_{stp}/(min\ mmHg)$ |
| $DM_{CO}$; $DM_{NO}$ | Diffusive conductance for CO and NO in $ml_{stp}/(min\ mmHg)$ |
| Hb | Haemoglobin molecule |
| $Hct$ | Haematocrit |
| $L_M$; $L_P$ | Thickness of membrane; plasma in μm |
| $L_{RBC}/2$ | Half thickness of a flat RBC in μm |
| $L_D$ | Penetration depth in μm |
| $N_{RBC}$ | Number of RBC in the lung |
| $P_{O2}$ | Oxygen partial pressure in mmHg |
| RBC | Red blood cell |
| RF | First initials of Roughton and Forster |
| $r_a$; $r_b$ | Long and short radius of the biconcave RBC in μm |
| $r_{RBC}$ | Radius of the spherical RBC in μm |
| $S$ | Total gas exchange surface in $m^2$ |
| $S_{RBC}$ | RBC surface area in $\mu m^2$ |
| TD | Time-dependent (or time-based) interpretation |
| $dV$ | Small volume element in RBC |
| $Vc$ | Pulmonary capillary volume in ml |
| $V_{RBC}$ | Volume of a red blood cell in $\mu m^3$ |
| $W$ | Half distance between periodic RBCs in μm |
| $\alpha_{CO}$; $\alpha_{NO}$ | Gas to liquid partition ratio for CO and NO (dimensionless) |
| $\phi$ | Molecular flux per unit time in $s^{-1}$ |
| $\theta$ | Specific transfer conductance of gas species in blood |
| $\tau_{CO}$; $\tau_{NO}$ | Characteristic reaction times for CO and NO with Hb molecules in millisecond |

chemical kinetics studies (Gibson et al., 1955; Chakraborty et al., 2004; Kang and Sapoval, 2016).

In contrast to the micro-dynamics discussed above, a *global and steady state* interpretation has been proposed by Roughton and Forster (1957) hereafter called RF. It is expressed by the RF equation:

$$\frac{1}{DL_{CO}} = \frac{1}{DM_{CO,RF}} + \frac{1}{\theta_{RF} \cdot Vc_{RF}} \tag{2}$$

where $DL_{CO}$ is the lung diffusing capacity for CO (the quantity that is measured), $1/DM_{CO,RF}$ is called the diffusive resistance, $\theta_{RF}$ is the "specific blood conductance" and $Vc_{RF}$ is the pulmonary capillary volume. The index RF is kept here because we will compare these quantities with their mathematical equivalents below.

The Roughton and Forster interpretation is the dominant model used by the scientific and clinical communities. The physical interpretation of this scheme is that the global lung capture resistance ($1/DL_{CO}$) is the sum of two resistances in series, the diffusive resistance that is supposed to characterize the transfer from the gas to the external surfaces of the RBCs, and the blood resistance related to diffusion and reaction inside RBCs. The RF interpretation is the standard in this field (see Hughes and Bates, 2003 for a review) and it is used in published recommendations for CO and NO lung function testing (MacIntyre et al., 2005). Since the late 1950′s up to the present there have been a number of contributions that examine both experimentally and theoretically this interpretation in different situations (Hughes and Pride, 1999).

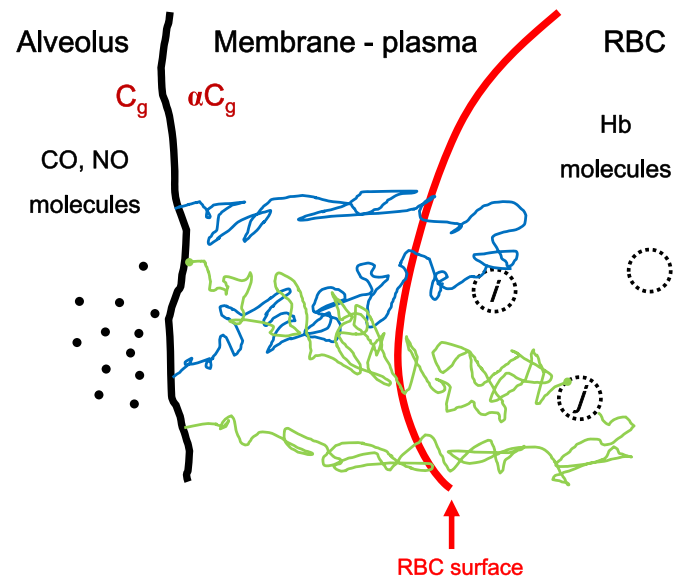


**Fig. 1.** Schematic representation of the capture process. The gas concentration $C_g$ drops through extremely rapid dissolution to $\alpha C_g$ on the internal face of the alveolar-capillary interface (α is the dimensionless gas to liquid partition ratio). Then the molecules from any starting point on the interface move along random individual paths (Brownian diffusion) through the membrane and plasma and into the RBC cytoplasm to reach the Hb molecules and finally react. This random transport is represented by the blue and green trajectories. Figure from Kang and Sapoval (2016).

Such a simplified description of this complex phenomenon by two independent resistances requires as a necessary (but not sufficient) condition that the periphery of a RBC is at a uniform concentration (iso-concentration) and be the same for all the RBCs. For general RBC morphology (and situations where these cells are moving in the capillaries, taking different shapes through time and even forming clusters), this condition is not satisfied.

It should be recalled that the RF equation does not arise from a general solution of the mathematical problem illustrated in Fig. 1. So, the fundamental question remains, how does diffusion and reaction interact and contribute to the global capture? The answer to that question is important because a $DL_{CO}$ measurement, if interpreted by RF, depends on three unknown parameters, $Vc_{RF}$, $DM_{RF}$, and $\theta_{RF}$. This renders the determination of the pertinent physiological quantities $DM_{RF}$ and $Vc_{RF}$ dependent on the *choice* of $\theta_{RF}$. Different approaches to this choice are discussed in the literature (see for instance the references in Coffman et al., 2016).

Roughton and Forster were conscious of this difficulty and they solved part of the problem by proposing the measurement of $DL_{CO}$ as a function of the oxygen partial pressure using the assumption that $1/\theta_{RF}$ is proportional to this pressure as suggested by their experiments. This was the invention of the RF extrapolation that allows, in principle, one to measure $DM_{CO,RF}$. Later, using the fact of a very rapid reaction rate of Hb with NO, Guénard et al. (1987) suggested that the measure of $DL_{NO}$ considered to be very close to $DM_{NO,RF}$ would give an approximate measure of $DM_{CO,RF}$ based on the scaling of $DL_{NO}$ from CO and NO solubilities and diffusivities using Graham's and Fick's laws.

Solving the problem illustrated in Fig. 1 is beyond the scope of a direct mathematical analysis. Nonetheless, the objective of this work is to examine simple cases where exact analytical or precise numerical values of $DL_{CO}$ and $DL_{NO}$ can be obtained. We will provide solutions to the diffusion-reaction equations for simplified and static boundary conditions. One can then check if their dependence on the reaction rate and capillary volume confirms the RF interpretation. Notwithstanding the simplifications here, the results show that the RF understanding of $DL_{CO}$ and $DL_{NO}$ is inaccurate. At the

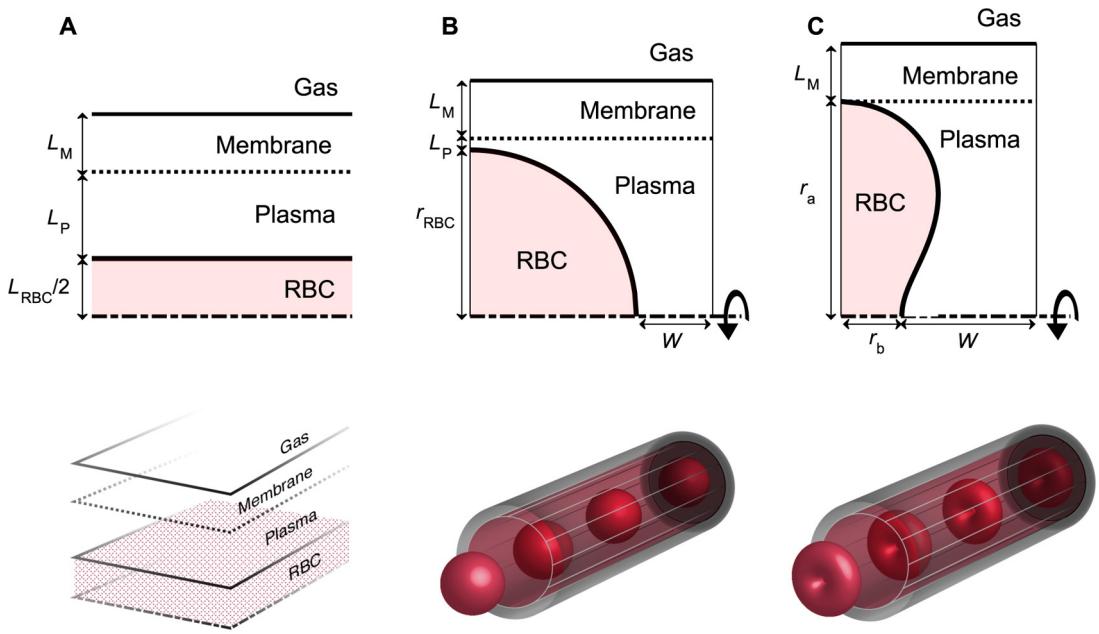


**Fig. 2.** Three geometries of gas-membrane-plasma-RBC structure. (Top) A: Flat parallel structure of a symmetrical gas-membrane-plasma-RBC geometry. B: Spherical RBCs inside a cylindrical capillary represented by the quarter of an axial planar cross-section. C: Biconcave RBCs in a cylindrical capillary represented by the quarter of an axial planar cross-section. (Bottom) 3D illustrations of each geometry.

same time, this study opens a new perspective for a better interpretation of these quantities.

Since this study is directed towards the pulmonary physiology community, the details of the calculations will be given in appendices and the results will be illustrated through graphs. The role of mathematics here is not to give results that could directly be applied to clinical questions but to help to select between the methods of interpretation those that are better founded.

## 2. Methods

During the single-breath (and hold) diffusing capacity manoeuvre, the gas molecule concentration inside the RBC $C_I$ follows the diffusion-reaction equation:

$$\frac{\partial C_I(x,y,z,t)}{\partial t} = D\left(\frac{\partial^2 C_I(x,y,z,t)}{\partial x^2} + \frac{\partial^2 C_I(x,y,z,t)}{\partial y^2} + \frac{\partial^2 C_I(x,y,z,t)}{\partial z^2}\right) - \frac{C_I(x,y,z,t)}{\tau} \quad (3)$$

where $D$ is the molecular diffusivity in the cytoplasm (taken here as the value in plasma). It is an exact and general mathematical result that the solution of the time-dependent Eq. (3) is the sum of a steady-state but space-dependent solution and a series of time decaying exponentials where the slowest term has a characteristic decay time of order $L^2/D$ where $L$ is the size of the system. For usual $D$ values and $L$ of order 1 μm, this time constant is of the order of 1 millisecond. This means that after a few milliseconds the solution of the time-dependent Eq. (3) is, to a very good approximation, the time-independent but space-dependent function. The complete time dependent solution will be discussed in the Section 3.3.

Inside the RBC, the steady state solution satisfies the time-independent equation

$$D\left(\frac{\partial^2 C_I(x,y,z)}{\partial x^2} + \frac{\partial^2 C_I(x,y,z)}{\partial y^2} + \frac{\partial^2 C_I(x,y,z)}{\partial z^2}\right) - \frac{C_I(x,y,z)}{\tau} = 0 \quad (4)$$

In the membrane plus plasma region (i.e., outside the RBC with no haemoglobin molecules), the external concentration $C_E$ obeys the simple steady-state diffusion or Laplace equation:

$$\left(\frac{\partial^2 C_E(x,y,z)}{\partial x^2} + \frac{\partial^2 C_E(x,y,z)}{\partial y^2} + \frac{\partial^2 C_E(x,y,z)}{\partial z^2}\right) = 0 \quad (5)$$

The gas concentration must also obey boundary conditions: The concentration on the internal interface of the capillary is equal to $\alpha C_g$ and the concentrations and fluxes are continuous at the RBC periphery:

$$\left(C_E = \alpha C_g\right)_{\text{capillary periphery}}; \qquad (C_E = C_I)_{\text{RBC periphery}}; \qquad \left(\frac{dC_E}{dn} = \frac{dC_I}{dn}\right)_{\text{RBC periphery}} \quad (6)$$

where $n$ is the normal to the RBC periphery. The continuity of the derivatives is linked to the fact that the diffusivities in plasma and the RBC cytoplasm can be considered to be approximately equal. This point is not trivial as the interior of RBCs is crowded by haemoglobin molecules that occupy about 30% of the volume. It is well known that in such a situation, like in porous materials, diffusion at short distances (or short time) is not perturbed while long distance diffusivity is reduced. A recent detailed study of diffusion in crowded systems (Palombo et al., 2013) showed that when applied to the RBC situation, for distances of order the RBC size, diffusivity is still within a good approximation the diffusivity in plasma or water. Note that the diffusivities measured in solutions which have been recently used in this field (Sakai et al., 2008; Azarov et al., 2011; Borland et al., 2014) are *long distance* diffusivities. Until now, there exists no measurement of NO diffusivity in concentrated Hb solution with thicknesses of order 1 μm, which would show that the short distance diffusivity is larger than the long distance value.

Eqs. (4)–(6) define the minimal mathematical description of the capture problem, i.e., a diffusion-reaction in two different media: a purely diffusion zone limiting a diffusion-reaction region.

Diffusivity values of CO and NO found in the literature are varied (see the Appendix A of Kang and Sapoval, 2016 and the refer-

**Table 1**
Values of geometrical parameters.

| A. Flat parallel structure | B. Spherical RBC | C. Biconcave RBC |
|---|---|---|
| $L_M = 1\ \mu m$ | $L_M = 1\ \mu m$ | $L_M = 1\ \mu m$ |
| $L_P = 1.5\ \mu m$ | $L_P = 0.2\ \mu m$ | $r_a = 3.72\ \mu m$ |
| $L_{RBC}/2 = 1\ \mu m$ | $r_{RBC} = 2.88\ \mu m$ | $r_b = 0.90\ \mu m$ |
| | $W = 1.32\ \mu m$ | $W = 1.98\ \mu m$ |

Cell geometries are chosen to have the volume of RBC $V_{RBC} = 100\ \mu m^3$. $L_P$ and $W$ correspond to a haematocrit $Hct = 40\%$.

ences therein). Many studies have used Graham's law to obtain $D_{NO}/D_{CO}$ but Graham's law has been proved for gases not for liquids. The problem of diffusivities in liquids is complex. First Graham's law, stating that the gas diffusion is inversely proportional to the square root of its molecular weight M, has been demonstrated for gases only. In liquids there is also a square root of M, but it is far from being the dominant difference between these species. And among the other physical reasons for different diffusivities, the fact that CO and NO are polar molecules that carry different electric dipole moments plays a role. These different electric moments for CO and NO couple with water molecule dipole moments differently. This is a complex microscopic phenomenon in liquids. For this reason, one has to rely on *experimental* measurements. In this study, we use the interpolated values for 37 °C from Wise and Houghton (1968): $D_{CO} = 3.26 \times 10^{-5}\ cm^2/s$, $D_{NO} = 4.80 \times 10^{-5}\ cm^2/s$ and $D_{NO}/D_{CO} = 1.47$. (Wise and Houghton measured NO and CO diffusivity by following the rate of collapse of bubbles in gas-free water. Their results should then be considered as an approximate assumption for plasma and lung tissues.)

The reaction time $\tau_{CO}$ of CO with Hb in RBC can be obtained from chemical kinetics. Kang and Sapoval (2016) deduced previously that $\tau_{CO} = 0.5$ ms for 100 mmHg of oxygen partial pressure and that, for larger $O_2$ partial pressures, $\tau_{CO}$ is linearly proportional to the pressure. The NO reaction time $\tau_{NO}$ is of order 5 microseconds, i.e., it is shorter than $\tau_{CO}$ by two orders of magnitude (Sakai et al., 2008). The partition ratios $\alpha_{CO} = 0.018$ and $\alpha_{NO} = 0.041$ (Cotes et al., 2006) were used.

Three different geometries of gas-membrane-plasma-RBC structures are considered in this study (Fig. 2). A: flat parallel structures; B: spherical RBCs in a cylindrical capillary; C: biconcave RBCs in a cylindrical capillary.

Eqs. (4)–(6) were solved for each case with values of geometrical parameters given in Table 1. The analytical solution for case A is given in Appendix A. As there is no analytical solution for cases B and C, numerical computations based on the Finite Element Method (FEM) were used (see the Appendix B).

## 3. Results and discussion

To qualitatively understand the results, one should recall the notion of "penetration depth during the reaction time", which measures the order of the distance over which diffusing molecules react and disappear. Consider, for example, a planar source at concentration $C_0$ in contact with a diffusion-reaction medium with diffusivity $D$ and reaction time $\tau$. The solution of Eq. (4) is a function of the distance $x$ to the source of the form $C = C_0 \exp(-x/(D\tau)^{1/2})$. This means that the molecules penetrate the reacting medium to a depth of order $(D\tau)^{1/2}$ before reacting. For this reason, the length

$$L_D = \sqrt{D\tau} \tag{7}$$

is called the penetration depth.

For the case A, the spatial distribution of the concentration computed using Eqs. (A.4)–(A.8) is shown in Fig. 3. One observes that the reaction time determines the penetration depth. For CO, one obtains $L_{D,CO} = (D_{CO}\tau_{CO})^{1/2} \approx 1\ \mu m$, which is of order of a typical RBC

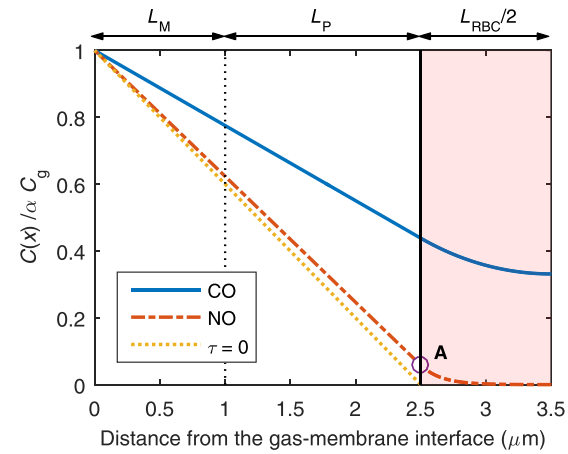


**Fig. 3.** Spatial concentration distribution of CO (blue) and NO (red). The figure represents a half symmetrical planar RBC membrane plasma geometry. The vertical axis represents the concentration normalized to the concentration at the internal interface of the gas-membrane frontier. The dotted line represents the concentration distribution in the limiting case $\tau = 0$. The point A shows normalized concentration of NO at the RBC surface. These results have been calculated from Eqs. (A.4)–(A.8).

half width. For NO, one obtains $L_{D,NO}$ of order 0.1 μm as illustrated in the figure. This justifies the qualitative statement that CO capture is a bulk effect whereas NO capture is a "surface absorption". One should stress however that there is a small but finite penetration of NO molecules into the RBC volume.

The fact that the slope of dot-dashed line is slightly smaller than that of the dotted line is the consequence of the small penetration of NO inside the RBC space. The diffusive flux is proportional to the slope of the straight line in the membrane/plasma region. For infinite reaction rate or $\tau = 0$ (dotted curve) the flux is proportional to $1/(L_M + L_P)$ and the resistance $R$ is proportional to $(L_M + L_P)$. For NO, equating the flux $(1\text{-}C(L_M + L_P)/\alpha C_g)/(L_M + L_P)$ to the internal flux $(C(L_M + L_P)/\alpha C_g)/L_D$ by continuity on the RBC membrane at point A in Fig. 3, one can compute the increase in apparent resistance $\Delta R/R = L_D/(L_M + L_P)$ in accordance with the data of Fig. 3. Note that this resistance increase is not due to any anomalous resistance from the RBC morphology as suggested by Borland et al. (2010, 2014) and Vaughn et al. (2000) but merely due to finite penetration before reaction.

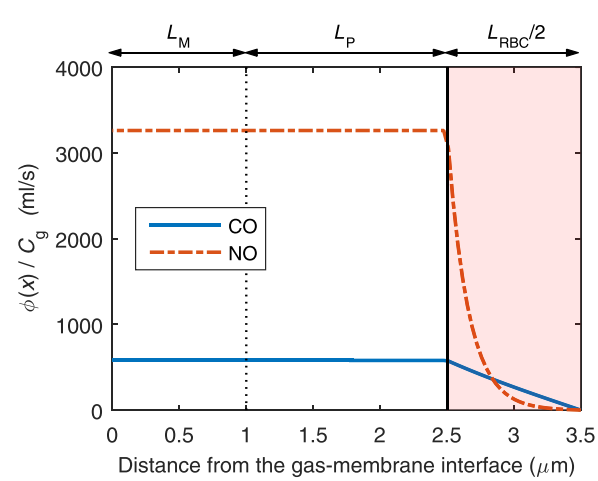


**Fig. 4.** Spatial distribution of the diffusive flux. The vertical axis represents ratio of the diffusive flux to the alveolar gas concentration. The flux is constant up to the RBC surface because there is no reaction there.

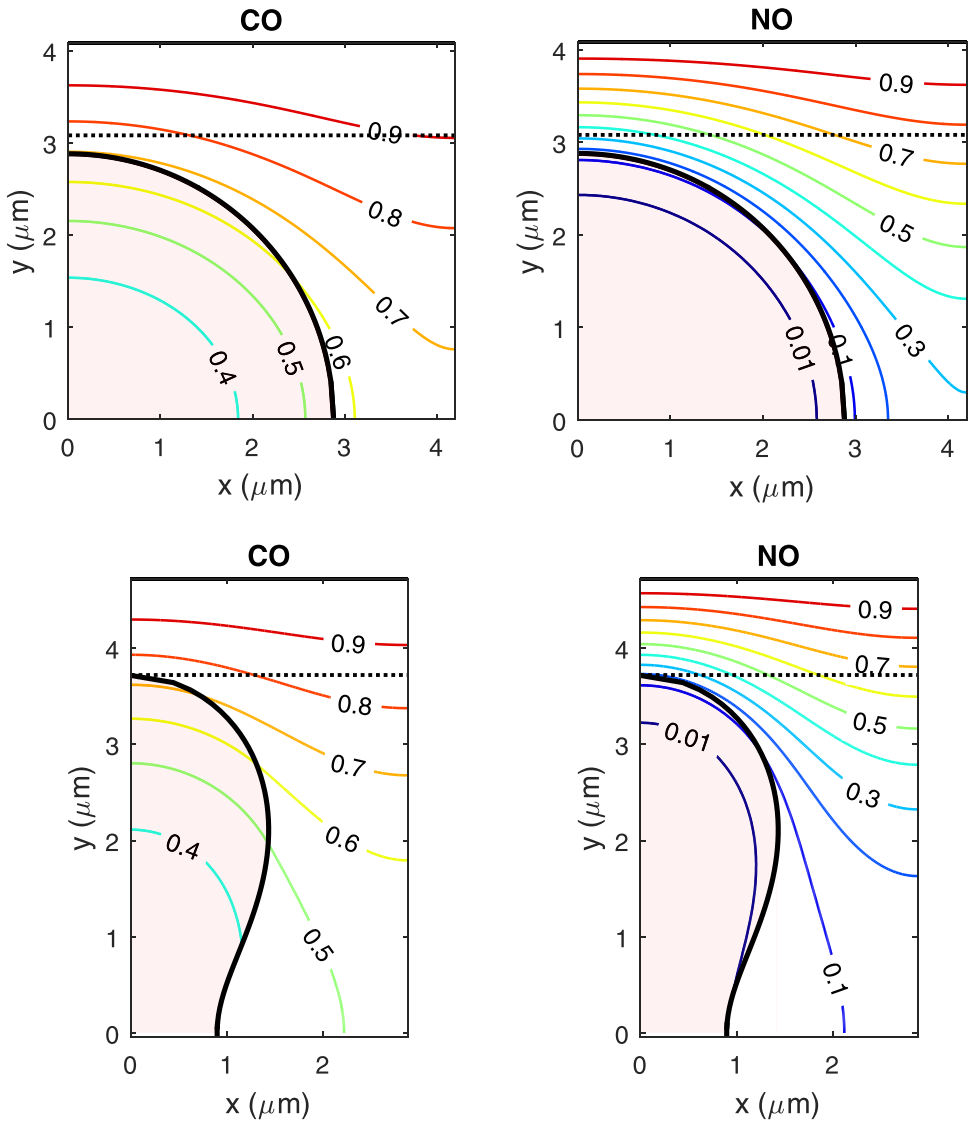


**Fig. 5.** Spatial distribution of CO and NO concentrations for equi-distant RBCs. Top and bottom correspond to spherical and biconcave RBCs. The figure represents one fourth of an RBC axial planar cut inside the cylindrical capillary of Fig. 2. The colored lines are the loci of isoconcentration with values decreasing from 1 on the upper thick line. The dotted line represents the membrane-plasma interface. The data correspond to Hct = 0.4.

The spatial distribution of the diffusive flux is given by Fick's law

$$\phi(x) = -DS\frac{dC(x)}{dx} \tag{8}$$

where $S$ is the total gas exchange surface. One can write $S = N_{RBC} \times S_{RBC} = (VcHct/V_{RBC}) \times S_{RBC}$ where $N_{RBC}$ is the number of RBCs in diffusive contact with the gas, $Vc$ is the pulmonary capillary volume, $Hct$ is haematocrit and $V_{RBC}$ and $S_{RBC}$ are the RBC volume and surface area, respectively. In this artificial morphology, a RBC is supposed to be a square box of thickness $L_{RBC} = 2\,\mu m$ and $V_{RBC} = 100\,\mu m^3$ giving $S_{RBC} = 100\,\mu m^2$. With $VcHct = 44\,cm^3$ (Kang and Sapoval, 2016), one obtains $S = 44\,m^2$. The spatial distribution of the diffusive flux is shown in Fig. 4.

The diffusing capacity DL can be deduced from the global flux which is given by the derivative of the concentration at the gas-membrane interface (see Eqs. (A.9) and (A.11)):

$$\frac{1}{DL} = \frac{1}{\frac{DS\alpha}{L_M+L_P}} + \frac{1}{\frac{DS\alpha}{L_D}\tanh\left(\frac{L_{RBC}/2}{L_D}\right)} \tag{9}$$

where $\tanh(x) = (1\text{-}\exp(-2x))/(1+\exp(-2x))$ is the hyperbolic tangent function. In the usual physiological units, we obtain

**Table 2**
Computation results for the three morphologies.

| Case | | A (Flat) | B (Sphere) | C (Biconcave) |
|---|---|---|---|---|
| $DL_{CO}$ (ml/min/mmHg) | | 46 | 63 | 62 |
| $DL_{NO}$ (ml/min/mmHg) | | 258 | 537 | 544 |
| $DL_{NO}/DL_{CO}$ | | 5.6 | 8.6 | 8.8 |
| $DL_{CO}$ for $\tau = 0$ | True | 82 | 184 | 188 |
| (ml/min/mmHg) | Extrapolation | 72 | 128 | 124 |
| | Scaling from DLNO | 77 | 160 | 161 |

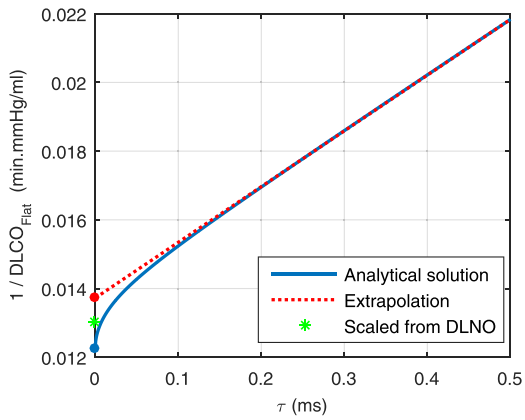


**Fig. 6.** Roughton and Forster plot of $(1/DL_{CO})_{exact}$ for case A as a function of the reaction time ($\tau$ is proportional to $P_{O2}$ for $P_{O2} > 80$ mmHg). Note that the "Scaled from $DL_{NO}$" is a value of $1/DL_{CO}$ for $\tau_{CO} = 0$ that is deduced from $DL_{NO}$ using the ratio 3.35 in Eq. (12).

$DL_{CO} = 46$ ml/min/mmHg, $DL_{NO} = 258$ ml/min/mmHg, and the ratio $DL_{NO}/DL_{CO} = 5.6$.

For NO capture with its very short reaction time, the penetration length $L_D$ is much smaller than $L_{RBC}/2$, so that $\tanh[(L_{RBC}/2)/L_D]$ is close to 1, and Eq. (9) can be simplified to

$$\frac{1}{DL} = \frac{L_M + L_P + L_D}{DS\alpha} \tag{10}$$

The results for the cases B and C are obtained numerically using a finite element method (FEM) (see the Appendix B). The spatial distributions of CO and NO concentrations are shown in Fig. 5.

For CO, one observes that no isoconcentration line matches the RBC periphery. One also notes that a large fraction of the RBC volume is engaged in capture as illustrated by the isolines in Fig. 5 that vary weakly over the RBC volume. This is due to the value of the penetration depth for CO which is close to 1 μm. In this sense, $DL_{CO}$ measures a "volume absorption".

On the contrary, the concentration of NO is very small inside the RBC. Only a very small fraction of the RBC volume is working as illustrated by the isolines in Fig. 5 that vary very rapidly over the RBC volume. This is due to the small value of the penetration depth for NO which is at most 0.1 μm. In that sense $DL_{NO}$ measures approximately a "surface absorption". A pure surface absorption would correspond to $\tau = 0$.

The values of $DL_{CO}$ and $DL_{NO}$ in the three configurations studied above are summarized in Table 2.

The results above, although describing simplified geometries, are mathematically exact for case A and very precise for cases B and C. They deal with the simplest version of the physico-chemical phenomena involved in the capture of gases by haemoglobin, namely diffusion and reaction. Comparing the results and the RF interpretation leads us to discuss the following points.

### 3.1. The Roughton and Forster extrapolation: a problem?

The Roughton and Forster extrapolation can be compared with the calculated solution of the dependence of $1/DL_{CO}$ on the reaction time. For case A shown in Fig. 6 and Table 2, one finds that the *linearly extrapolated value* of $DL_{CO}$ is *different* from the exact $DL_{CO}(\tau = 0)$.

The important point here is not the size of the discrepancy between these two values *but that they are both exact*. One can deduce the extrapolation error from the analytic calculation in Appendix A

$$err = \frac{L_{RBC}/2}{3\,(L_M + L_P)} \tag{11}$$

which gives 13% of error for this particular geometry.

For cases B and C, one observes the same type of discrepancy but the difference is significantly larger as shown in Fig. 7 and Table 2. For all the geometries studied in the present work $1/DL_{CO}$ versus $\tau$ is only approximately linear and the extrapolation does not give the expected $1/DL_{CO}$ at $\tau = 0$. Thus, this defect of the RF extrapolation is conceptual.

The above graphs are not given as a function of $P_{O2}$ but as a function of the reaction time which is known to be proportional to $P_{O2}$ for large enough $P_{O2}$ (see Kang and Sapoval, 2016). The case $\tau = 0$ cannot be reached because even totally desaturated Hb molecules would react with a finite reaction rate. Although the chemical kinetics of haemoglobin are complex (Gibson et al., 1955; Forster, 1987) one can say that the reaction time decreases when the number of reactive Hb molecules increases. In this way the reaction time should roughly decrease with $P_{O2}$ as $(1-\text{Saturation}(P_{O2}))^{-1}$, i.e. at least one order of magnitude from 100 mmHg. But even if very small values of $\tau_{CO}$ cannot be reached experimentally, $DM_{CO}$ is still well defined as the limit of $DL_{CO}$ for $\tau_{CO} = 0$. Conversely, this allows one to consider that experimental $DL_{NO}$ is close to the true $DM_{NO}$.

In addition, both CO and NO obey the same Eqs. (4)–(6) with the different partition ratios and solubilities. In both hypothetical cases

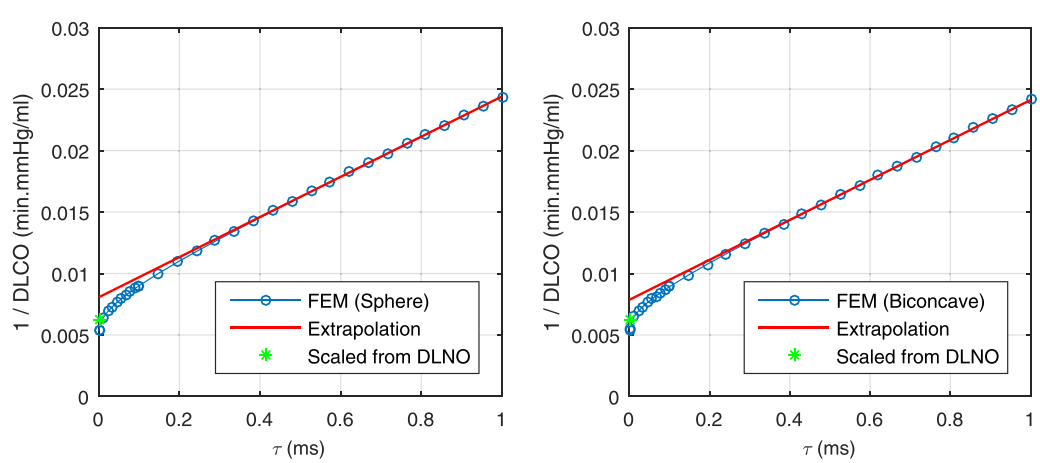


**Fig. 7.** RF extrapolation for spherical (left) and biconcave (right) RBCs. Three $1/DL_{CO}$ values at $\tau = 0$ need to be compared: from FEM, from extrapolation and from scaling. Note that the "Scaled from $DL_{NO}$" is a value of $1/DL_{CO}$ for $\tau_{CO} = 0$ that is deduced from $DL_{NO}$ using the ratio 3.35 in Eq. (12).

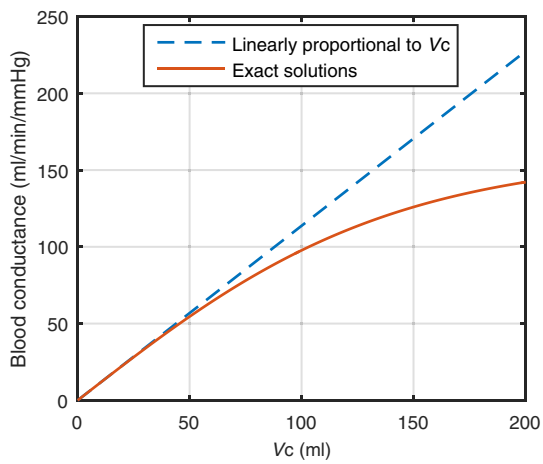


**Fig. 8.** Dependence of the blood conductance on *Vc*. The dashed line is a tangent of the exact solutions for small *Vc*. In the RF interpretation, the blood conductance is linearly proportional to *Vc*, while the hyperbolic tangent of the exact solution is non-linear. Their difference increases with *Vc*.

$\tau_{CO} = 0$ and $\tau_{NO} = 0$ the corresponding diffusive capacities $DL_{NO}$ and $DL_{CO}$ would scale simply as

$$\frac{DM_{NO}}{DM_{CO}} = \frac{DL_{NO}(\tau_{NO} = 0)}{DL_{CO}(\tau_{CO} = 0)} = \frac{\alpha_{NO}}{\alpha_{CO}}\frac{D_{NO}}{D_{CO}} = 3.35 \quad (12)$$

For physical reasons these quantities cannot be measured but due to the small value of $\tau_{NO}$, one can use relation (12) to predict an approximate value for $DL_{CO}(\tau_{CO} = 0)$ from the experimental value of $DL_{NO}$ with a finite but small $\tau_{NO}$. This value is shown in Figs. 6 and 7 by the green stars. As expected, these values are approximate, but the approximation is fairly good for all three cases.

### 3.2. *Vc dependence*

Comparing Eq. (9) and the RF Eq. (2) shows that in case A the exact solution consists of the contribution of two resistances: the first term in the right hand side of Eq. (9) corresponds to the membrane resistance and the second corresponds to the blood part of RF. That is, *for this very simple geometry*, the RBC surface is at iso-concentration due to symmetry. Fig. 5 shows that the RBC surface and iso-concentration lines do not coincide in the other cases.

More importantly, the so-called blood conductance is now a hyperbolic tangent function of $L_{RBC}$, i.e., a nonlinear function of *Vc* as written below:

$$\text{Blood conductance} = \frac{DS\alpha}{L_D}\tanh\left(\frac{L_{RBC}/2}{L_D}\right) = \frac{DS\alpha}{L_D}\tanh\left(\frac{Vc \cdot Hct}{S \cdot L_D}\right) \quad (13)$$

This exact result shows that the blood conductance *is not* linearly proportional to *Vc* in contradiction with RF. This is illustrated in Fig. 8. The direct comparison shows the exact solution and RF interpretation exhibit different behaviours as a function of *Vc even* in the idealized case of a flat RBC surface, which is an isoconcentration. The qualitative understanding of the exact result is that if the penetration depth $L_D$ is smaller than *Vc*, molecules do not penetrate the entire volume of the RBC.

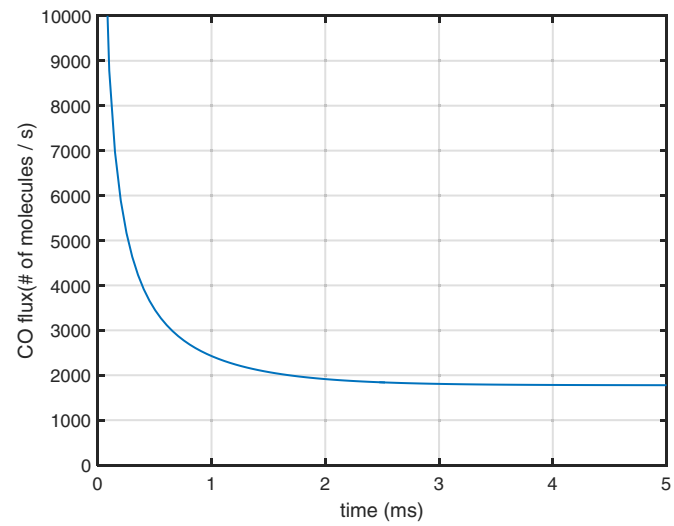


**Fig. 10.** Time evolution of the CO flux per RBC. Note that the steady-state is reached within 3 ms.

### 3.3. *Steady state capture versus complete time-dependent capture*

To make it clear that the capture is essentially governed by the steady state regime, one can compute the solution of the full time dependent diffusion reaction Eq. (3). The results are shown in Fig. 9, which presents concentration distributions at different times for a biconcave RBC. It is clear that the steady-state is reached within a few milliseconds after the RBC is in diffusive contact with the gas. More importantly, it should be noted that after that time *there is no advancing front*.

The global flux time dependence is shown in Fig. 10.

## 4. Summary and conclusion

In this work, three cases of RBC morphology have been used to investigate the Roughton and Forster interpretation of $DL_{CO}$ and $DL_{NO}$. The analysis deals with the minimal model of the physico-chemical phenomena involved in the capture of gases by haemoglobin, namely diffusion and reaction. The results, obtained

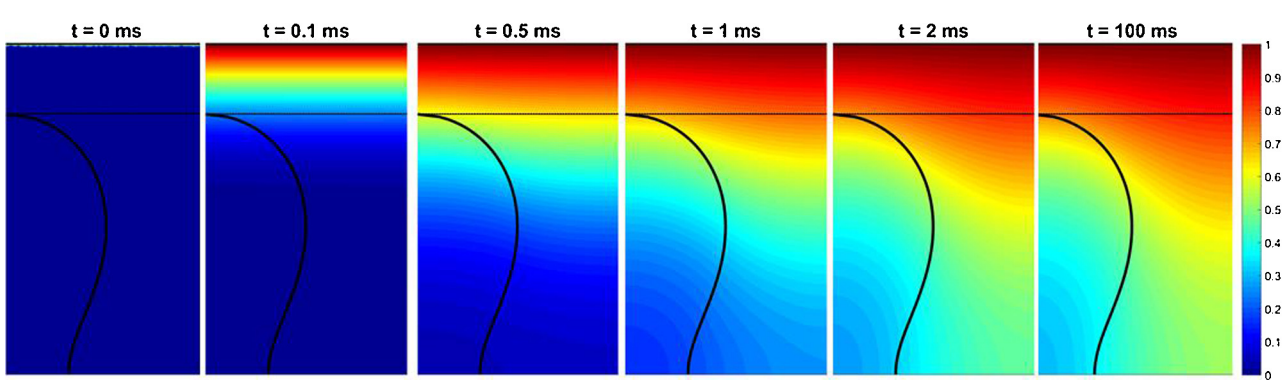


**Fig. 9.** Time evolution of the spatial distribution of CO concentration where t represents the time after the RBC is in diffusive contact with the gas. Concentrations are normalized to the concentration at the gas-membrane interface $\alpha C_g$. The horizontal line represents the membrane-plasma interface.

with different morphologies, have common properties and then provide insight into the conceptual basis of the transfer process.

First of all, we emphasize that the *experimental* quantities $DL_{CO}$ and $DL_{NO}$ should not be confused with the "conceptual quantities" $DM_{CO,RF}$ and $DM_{NO,RF}$ invented by Roughton and Forster. They are conceptual in the sense that they have never been measured as such. Their *supposed* correspondence is $DM_{CO,RF} = DL_{CO}(\tau_{CO} = 0)$ and $DM_{NO,RF} = DL_{NO}(\tau_{NO} = 0)$ but this condition is never realized experimentally.

The principal conclusions of the paper are:

- $1/DL_{CO}$ versus $\tau co(P_{O2})$ is *only approximately* linear. Consequently, the linear RF extrapolation method *does not give* $1/DL_{CO}(\tau_{CO} = 0)$. Therefore, the relation $DM_{CO,RF} = DL_{CO}$(extrapolated to $PO_2 = 0$) is erroneous.
- The dependence of $DL_{CO}$ on the capillary volume *Vc* does not fit the RF prediction, even for an idealized flat case where the RBC surface is an isoconcentration.
- The value of $DL_{NO}$ implies a small but finite participation of the interior of the RBC *that behaves like an internal resistance*. Thus, $DL_{NO}$ is a good approximation of $DM_{NO}$ (within a few per cent) from which one could deduce $DM_{CO}$. However, there is no use of $DM_{CO}$if it is recognized that the RF equation is inadequate to describe CO capture.

Not mentioned in this paper is the case of spherical vesicles containing Hb molecules for which exact analytical computation can also be obtained. They exhibit the same properties that were discussed here for the different morphologies. They will be compared with experiments by Sakai et al. (2008) and Azarov et al. (2011) in a following paper.

One could ask about the influence of the values of the diffusivities used above on the conclusions and especially on the main conclusion that the real $DM_{CO}$ is different from the extrapolated $DL_{CO}$. To check this influence, the same calculations have been performed using an internal diffusivity of 1/3 of the external diffusivity. The results are summarized in the Appendix C. They show clearly that the fact that the extrapolated value is different from the real value for $\tau = 0$ is independent of the diffusivity values.

These conclusions constitute a somewhat negative view of $DL_{CO}$ measurements as interpreted through the RF equation. In fact, it is possible that $DL_{CO,}$ as currently used in lung function tests, have been partly misinterpreted in the past. Nevertheless, besides their interpretation, the accumulated clinical correlations between experimental $DL_{CO}$ values have their own validity. In such a situation where the current RF method appears to be misleading, one should consider a different method which itself has to be checked on the same geometries. This is the Time-Dependent approach, recently introduced by Kang and Sapoval (2016). This new way of understanding will be discussed in a forthcoming paper.

But the same results also lead to a new and different point of view about the clinical use of these lung function tests. The new point of view is to consider $DL_{CO}$ and $DL_{NO}$ as two *complementary* quantities that stand for themselves. $DL_{CO}$ measures a "volume absorption" that gives an indication about the haematocrit. $DL_{NO}$ measures a "surface absorption" and gives indication about the morphology of the space separating the alveolar membrane and plasma from the RBCs. As shown in Kang and Sapoval (2016), a specific interesting aspect of $DL_{NO}$ is that it presents a better sensitivity to membrane heterogeneity than $DL_{CO}$.

Besides that, the present work sheds new light on the discussions about $DL_{NO}$ in this special issue of RESPNB and the arguments presented in Zavorsky et al. (2017). First, suppose as generally admitted that $DL_{NO}$ is close to $DM_{NO}$ because the reaction rate of NO with Hb is very large. Then, if this is true, one should find the real $DM_{CO}$ through a simple scaling using the solubility and diffusivity of the respective species. The problem lies in the fact, reported here, namely that the scaled $DL_{CO}$ ($\tau = 0$) obtained here is not equal to the $DM_{CO}$ linearly extrapolated from large pressures. Related to that dilemma, several studies have questioned the interpretation of $DL_{NO}$ itself as related to some anomaly in the capture of NO (for example, finite against infinite $\theta_{NO}$, anomalous diffusion in or out of the RBC membrane). But what has not been questioned so far is the very validity of the Roughton and Forster model which leads, as shown here, to an erroneous interpretation of the extrapolated $DL_{CO}$. In the new interpretation of $DL_{CO}$ by Kang and Sapoval (2016) this contradiction disappears.

## Conflict of interest

The authors declare no competing financial interests.

## Acknowledgments

The authors wish to thank C. Hsia, J.M.B. Hughes, L. Kiger and M. Marden for interesting discussions and S. Ceste for the 3D illustration. This work was partially supported by Air Liquide Santé International.

## Appendix A. Analytical solution of CO and NO capture in the case of flat parallel structures.

The solution for the case of the flat parallel structure (shown in Fig. 2) is independent of the *y* and *z* axes along the surfaces such that this is a 1D problem in the transverse (vertical) direction. Then, the diffusion-reaction equation in the internal region of the RBC is simply

$$D\frac{d^2C_I}{dx^2} - \frac{C_I}{\tau} = 0 \qquad \left(0 < x < L_{RBC}/2\right) \tag{A.1}$$

where *x* is the distance from the cell center. In the external zone of the RBC, one has

$$\frac{d^2C_E}{dx^2} = 0 \qquad \left(L_{RBC}/2 < x < L_{RBC}/2 + L_P + L_M\right) \tag{A.2}$$

In the coordinates of Fig. 2, the boundary conditions are

$$\begin{aligned} &C_E\left(L_{RBC}/2 + L_p + L_M\right) = \alpha C_g \\ &C_E\left(L_{RBC}/2\right) = C_I\left(L_{RBC}/2\right) \\ &\frac{dC_E\left(L_{RBC}/2\right)}{dx} = \frac{dC_I\left(L_{RBC}/2\right)}{dx} \end{aligned} \tag{A.3}$$

The linear solution of Eq. (A.2) is in the membrane-plasma space is

$$C_E(x) = A_E x + B_E \tag{A.4}$$

and the solution of Eq. (A.1) inside the RBC is

$$C_I(x) = A_I \cosh\frac{x}{L_D} + B_I \sinh\frac{x}{L_D} \qquad \left(\text{where} L_D = \sqrt{D\tau}\right) \tag{A.5}$$

where the cosh and sinh are the hyperbolic cosine and sine functions, respectively. From the system symmetry, $B_I = 0$. The length $L_D$ is the penetration depth characterizing qualitatively that diffusive molecules are absorbed on this length.

From the boundary conditions in Eq. (A.3), one obtains

$$A_I = \alpha C_g \frac{1}{\frac{L_M + L_P}{L_D}\sinh\frac{L_{RBC}/2}{L_D} + \cosh\frac{L_{RBC}/2}{L_D}} \tag{A.6}$$

$$A_E = \alpha C_g \frac{1}{L_D \coth\frac{L_{RBC}/2}{L_D} + L_M + L_P} \tag{A.7}$$

$$B_E = \alpha C_g \frac{L_D \coth \frac{L_{RBC}/2}{L_D} - L_{RBC}/2}{L_D \coth \frac{L_{RBC}/2}{L_D} + L_M + L_P} \tag{A.8}$$

These formulas fully determine the concentrations $C_E(x)$ and $C_I(x)$.

The flux of gas molecules is given by the product of diffusivity $D$, gas exchange surface $S$, and the derivative of $C_E(x)$:

$$\phi_E(x) = -DS\frac{dC_E(x)}{dx} = -DSA_E = -DS\alpha C_g \frac{1}{L_D \coth \frac{L_{RBC}/2}{L_D} + L_M + L_P} \tag{A.9}$$

i.e., the flux is constant in this zone since there is no reaction. The local diffusive component of the flux inside the RBC $\phi_I(x)$ is given by the following equation and illustrated in Fig. 4. Note that the abscissae of Figs. 3 and 4 in the text represent distance from the gas-membrane interface having the opposite direction of $x$.

$$\phi_I(x) = -DS\frac{dC_I}{dx} = -DS\alpha C_g \frac{\sinh \frac{x}{L_D}}{(L_M + L_P)\sinh \frac{L_{RBC}/2}{L_D} + L_D \cosh \frac{L_{RBC}/2}{L_D}} \tag{A.10}$$

From Eq. (A.9), one obtains $1/DL_{CO}$

$$\frac{1}{DL_{CO}} = \frac{C_{g,CO}}{|\phi_{E,CO}|} = \frac{L_{D,CO} \coth \frac{L_{RBC}/2}{L_{D,CO}} + L_M + L_P}{D_{CO}S\alpha_{CO}} \tag{A.11}$$

For small $y = (L_{RBC}/2)/L_{D,CO}$ (i.e., for large $\tau_{CO}$), Eq. (A.11) becomes

$$\frac{1}{DL_{CO}} \approx \frac{1}{D_{CO}S\alpha_{CO}}\left(L_M + L_P + \frac{D_{CO}\tau_{CO}}{L_{RBC}/2} + \frac{L_{RBC}/2}{3}\right) \tag{A.12}$$

where we used the series expansion of the hyperbolic cotangent:

$$\coth(y) = \frac{1}{y} + \frac{y}{3} - \frac{y^3}{45} + \ldots \tag{A.13}$$

The intercept of the RF extrapolation to $P_{O2} = 0$ ($\tau_{CO} \approx 0$) is

$$\frac{1}{DL_{CO}\left(\text{Ext.}P_{O_2} = 0\right)} = \frac{1}{D_{CO}S\alpha_{CO}}\left(L_M + L_P + \frac{L_{RBC}/2}{3}\right) \tag{A.14}$$

On the other hand, for large $y$, $\coth(y) \approx 1$, and Eq. (A.11) for $\tau_{CO} = 0$ becomes

$$\frac{1}{DL_{CO}(\tau_{CO} = 0)} \approx \frac{L_M + L_P}{D_{CO}S\alpha_{CO}} \tag{A.15}$$

Relative error of the extrapolation in Eq. (A.14) to the true value of $DM_{CO}$ in Eq. (A.15) is

$$err = \frac{L_{RBC}/2}{3(L_M + L_P)} \tag{A.16}$$

For the case that we consider in Fig. 3, $err = 13\%$ but it will vary according to the morphology.

## Appendix B. Numerical simulations.

The general form of the steady diffusion-reaction equation can be written as

$$D\Delta C - \frac{C}{\tau} = 0 \tag{B.1}$$

In 3D cylindrical coordinates, the Laplace operator $\Delta$ has the following form

$$D\left[\frac{1}{r}\frac{\partial}{\partial r}\left(r\frac{\partial C}{\partial r}\right) + \frac{1}{r^2}\frac{\partial^2 C}{\partial {\theta_r}^2} + \frac{\partial^2 C}{\partial z^2}\right] - \frac{C}{\tau} = 0 \tag{B.2}$$

Thanks to the symmetry of the cases B and C, there is no dependence on the angle $\theta_r$. Then, Eq. (B.2) can be reduced to

$$D\left[\frac{1}{r}\frac{\partial}{\partial r}\left(r\frac{\partial C}{\partial r}\right) + \frac{\partial^2 C}{\partial z^2}\right] - \frac{C}{\tau} = 0 \tag{B.3}$$

Eq. (B.3) has been solved with the Matlab PDE solver that uses the Finite Element Method (MathWorks, 2015). The steady diffusion equation has been converted with the same steps above and solved together with Eq. (B.3).

Biconcave RBC shape in case C can be defined as a locus of the points for which the product of distances to two fixed points is constant (Angelov and Mladenov, 2000). It is given by the equation

$$\left(x^2 + y^2 + a^2\right)^2 - 4a^2y^2 = c^4 \tag{B.4}$$

where $c^2$ is the constant corresponding to the product of the distances and $a$ is the half distance between the two points. In this study, $a = 2.55\ \mu m$ and $c = 1.06 \times a$ have been chosen to have approximately $100\ \mu m^3$ of RBC volume and desired concavity.

## Appendix C. Role of the internal diffusivity.

This Appendix answers the question of whether or not the conclusion, i.e., $1/DL_{CO}$ extrapolated to $\tau$=0 is different from $1/DL_{CO}$ ($\tau = 0$), depends on the diffusivity values to test that, we have conducted additional computations with $D_{NO} = D_{CO}$ and $D_{RBC,Internal} = 1/3 \times D_{RBC,External}$.

In comparison to Fig. 7, the values of $DL_{CO}$ in Fig. C1 are modified but the differences between the extrapolated values and the real values for $\tau = 0$ remain.

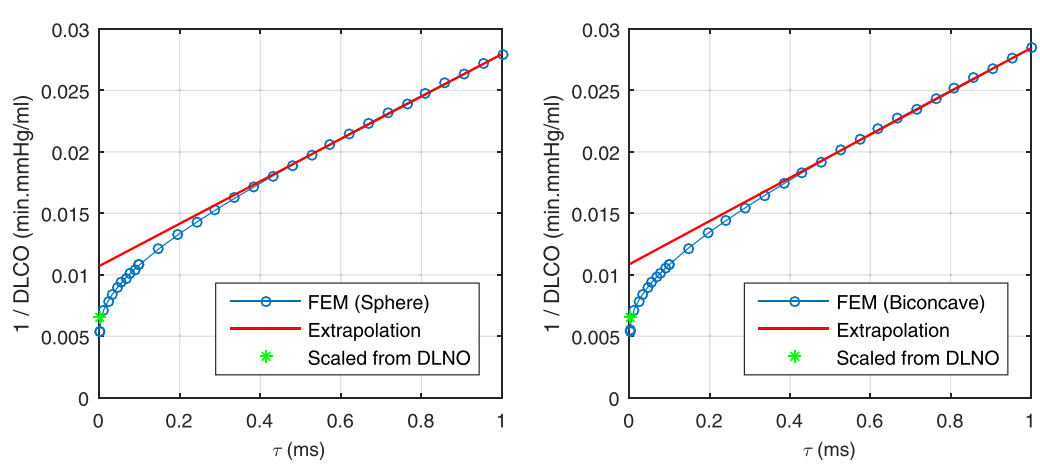


**Fig. C1.** RF extrapolation with different diffusivity inside and outside of RBC. (left) spherical RBC (right) biconcave RBC.

## References


Angelov, B., Mladenov, I.M., 2000. On the geometry of the red blood cell, geometry, integrability and quantization. In: Mladenov, I.M., Naber, G.L. (Eds.), Geometry, Integrability and Quantization. Coral Press, Sofia, pp. 27–46.

Azarov, I., Liu, C., Reynolds, H., Tsekouras, Z., Lee, J.S., Gladwin, M.T., Kim-Shapiro, D.B., 2011. Mechanisms of slower nitric oxide uptake by red blood cells and other hemoglobin-containing vesicles. J. Biol. Chem. 286, 33567–33579.

Borland, C.D.R., Higenbottam, T.W., 1989. A simultaneous single breath measurement of pulmonary diffusing capacity with nitric oxide and carbon monoxide. Eur. Respir. J. 2, 56–63.

Borland, C.D.R., Dunningham, H., Bottrill, F., Vuylsteke, A., Yilmaz, C., Dane, D.M., Hsia, C.C., 2010. Significant blood resistance to nitric oxide transfer in the lung. J. Appl. Physiol. 108, 1052–1060.

Borland, C.D.R., Bottrill, F., Jones, A., Sparkes, C., Vuylsteke, A., 2014. The significant blood resistance to lung nitric oxide transfer lies within the red cell. J. Appl. Physiol. 116, 32–41.

Chakraborty, S., Balakotaiah, V., Bidani, A., 2004. Diffusing capacity reexamined: relative roles of diffusion and chemical reaction in red cell uptake of $O_2$, CO, $CO_2$, and NO. J. Appl. Physiol. 97, 2284–2302.

Checchia, P., Bronicki, R., Goldstein, B., 2012. Review of inhaled nitric oxide in the pediatric cardiac surgery setting. Pediatr. Cardiol. 33, 493–505.

Coffman, K.E., Taylor, B.J., Carlson, A.R., Wentz, R.J., Johnson, B.D., 2016. Optimizing the calculation of DM, CO and VC via the single breath single oxygen tension DLCO/NO method. Respir. Physiol. Neurobiol. 221, 19–29.

Cotes, J.E., Chinn, D.J., Miller, M.R., 2006. Lung Function: Physiology, Measurement and Application in Medicine, sixth ed. Blackwell Publishing Ltd., pp. 224–229.

Foucquier, A., Filoche, M., Moreira, A.A., Andrade Jr., J.S., Arbia, G., Sapoval, B., 2013. A first principles calculation of the oxygen uptake in the human pulmonary acinus at maximal exercise. Respir. Physiol. Neurobiol. 185, 625–638.

Diffusion of gases across the alveolar membrane Forster, R.E. (Ed.), 1987. Handbook of Physiology. The Respiratory System. Gas Exchange, vol. IV. Am. Physiol. Soc., Bethesda, MD, pp. 71–88, sect. 3, chap. 5.

Frostell, C., Fratacci, M.J., Wain, J., Jones, R., Zapol, W., 1991. Inhaled nitric oxide. A selective pulmonary vasodilator reversing hypoxic pulmonary vasoconstriction. Circulation 83, 2038–2047.

Furchgott, R.F., Zawadzki, J.V., 1980. The obligatory role of endothelial cells in the relaxation of arterial smooth muscle by acetylcholine. Nature 288, 373–376.

Gibson, Q.H., Kreuzer, F., Meda, E., Roughton, F.J.W., 1955. The kinetics of human haemoglobin in solution and in the red cell at 37 °C. J. Physiol. 129, 65–89.

Griffiths, M., Evans, T., 2005. Inhaled nitric oxide therapy in adults. N. Engl. J. Med. 353, 2683–2695.

Guénard, H., Varène, N., Vaida, P., 1987. Determination of the lung capillary blood volume and membrane diffusing capacity in man by the measurements of NO and CO transfer. Respir. Physiol. 70, 113–120.

Hughes, J.M.B., Bates, D.V., 2003. Historical review: the carbon monoxide diffusing capacity (DLCO) and its membrane (Dm) and red cell (Θ•Vc) components. Respir. Physiol. Neurobiol. 138, 115–142.

Hughes, J.M.B., Pride, N.B., 1999. Lung Function Tests: Physiological Principles and Clinical Applications. Bailliere Tindall.

Ignarro, L.J., Byrns, R.E., Buga, G.M., Wood, K.S., 1987. Endothelium-derived relaxing factor from pulmonary artery and vein possesses pharmacologic and chemical properties identical to those of nitric oxide radical. Circ. Res. 61, 866–879.

Kang, M.-Y., Sapoval, B., 2016. Time-based understanding of DLCO and DLNO. Respir. Physiol. Neurobiol. 225, 48–59.

Kang, M.-Y., Katz, I., Sapoval, B., 2015. A new approach to the dynamics of oxygen capture by the human lung. Respir. Physiol. Neurobiol. 205, 109–119.

Krogh, M., 1915. The diffusion of gases through the lung of man. J. Physiol. 49, 271–296.

MacIntyre, N., Crapo, R.O., Viegi, G., Johnson, D.C., van der Grinten, C.P.M., Brusasco, V., Burgos, F., Casaburi, R., Coates, A., Enright, P., Gustafsson, P., Hankinson, J., Jensen, R., McKay, R., Miller, M.R., Navajas, D., Pedersen, O.F., Pellegrino, R., Wanger, J., 2005. Standardisation of the single-breath determination of carbon monoxide uptake in the lung. Eur. Respir. J. 26, 720–735.

Motterlini, R., Otterbein, L.E., 2010. The therapeutic potential of carbon monoxide. Nat. Rev. Drug Discov. 9, 728–743.

Palmer, R.M., Ferrige, A.G., Moncada, S., 1987. Nitric oxide release accounts for the biological activity of endothelium-derived relaxing factor. Nature 327, 524–526.

Palombo, M., Gabrielli, A., Servedio, V.D.P., Ruocco, G., Capuani, S., 2013. Structural disorder and anomalous diffusion in random packing of spheres. Sci. Rep. 3, 2631.

Roughton, F.J.W., Forster, R.E., 1957. Relative importance of diffusion and chemical reaction rates in determining rate of exchange of gases in the human lung, with special reference to true diffusing capacity of pulmonary membrane and volume of blood in the lung capillaries. J. Appl. Physiol. 11, 290–302.

Ryter, S.W., Choi, A.M., 2013. Carbon monoxide: present and future indications for a medical gas. Korean J. Intern. Med. 28 (2), 123–140.

Sakai, H., Sato, A., Masuda, K., Takeoka, S., Tsuchida, E., 2008. Encapsulation of concentrated hemoglobin solution in phospholipid vesicles retards the reaction with NO, but not CO, by intracellular diffusion barrier. J. Biol. Chem. 283, 1508–1517.

Vaughn, M.W., Huang, K.T., Kuo, L., Liao, J.C., 2000. Erythrocytes possess an intrinsic barrier to nitric oxide consumption. J. Biol. Chem. 275, 2342–2348.

Wise, D.L., Houghton, G., 1968. Diffusion coefficient of neon, krypton, xenon, carbon monoxide and nitric oxide in water at 10–60 °C. Chem. Eng. Sci. 23, 1211–1216.

Zavorsky, G.S., Hsia, C.C., Hughes, J.M., Borland, C.D., Guenard, H., van der Lee, I., Steenbruggen, I., Naeije, R., Cao, J., Dinh-Xuan, A.T., 2017. Standardisation and application of the single-breath determination of nitric oxide uptake in the lung. Eur. Respir. J. 49, 1600962.